Coupling X-ray Scattering and Nitrogen Adsorption: An Interesting Approach for the Characterization of Ordered Mesoporous Materials. Application to Hexagonal Silica

Pierre-Antoine Albouy*,† and André Ayral‡

Laboratoire de Physique des Solides, UMR CNRS 8502, Bâtiment 510, Université de Paris-Sud, F-91405 Orsay, France, and Institut Européen des Membranes, UMR CNRS 5635, CC047, Université Montpellier II, Place Eugène Bataillon, F-34095 Montpellier cedex 5, France

Received February 15, 2002. Revised Manuscript Received May 22, 2002

The structural evolution of a 2D hexagonal mesoporous silica powder during nitrogen adsorption at low temperature is followed by X-ray diffraction. The values for the pore radius and wall microporosity obtained with this technique compare well to the estimations drawn from volumetric measurements. It is further shown that capillary condensation is not accompanied by material shrinkage; on the contrary, a slight increase in the unit cell parameter is observed. A comparison of the diffracted intensity before gas adsorption and after capillary condensation allows the silica skeleton density to be estimated precisely. In the intermediate situation, intensity calculations are performed in the frame of a conventional model of a nitrogen film condensed on the mesopore walls; estimates of the film thickness are in good agreement with predictions. It is further possible to separate the evolution of the nitrogen content of the micro- and mesopores.

Introduction

Ordered mesoporous silicates can be synthesized using the templating effect of lyotropic mesophases formed by the self-assembly of surfactant molecules.[1] The 2D hexagonal type, labeled MCM41, is prepared by hydrothermal synthesis under basic conditions using cationic surfactants. It consists of hexagonally closed-packed cylindrical pores separated by silica walls. Sol−gel-derived thin layers[2−6] and powders[6] exhibiting a similar 2D hexagonal structure can also be obtained at room temperature and atmospheric pressure under neutral or preferably acidic conditions. Much work has been devoted to these materials, in particular for the precise characterization of their pore sizes from nitrogen adsorption−desorption measurements at 77.4 K.[7,8]

Scherer et al. showed previously that, in the case of highly porous silica aerogels (porosity ≈ 80−90%, pore volume ≈ 2−4 cm^3/g), the stresses associated with the capillary condensation of nitrogen in the pores can induce an important and partially irreversible contraction of the porous material.[9−11] It seems important to consider what happens during nitrogen capillary condensation in 2D hexagonal mesoporous silica (porosity ≈ 60−70%, pore volume ≈ 0.6−1.1 cm^3/g).

X-ray scattering is a powerful tool for characterizing the structure and texture of 2D hexagonal mesoporous silica.[12−14] If coupled with nitrogen adsorption, it should be a well-adapted method for following the dimensional variations of this ordered porous material from the evolution of its cell parameter. Moreover, because of the variation of the electron density, isotherm curves giving the evolution of the diffracted intensity as a function of the nitrogen relative pressure can be obtained, which can be used to investigate the porosity and to determine the size of the cylindrical pores.

Experimental Section

Sample Preparation. The 2D hexagonal silica powder was prepared using synthesis conditions previously optimized.[6] The silica precursor was tetraethoxysilane (TEOS, purity > 98%).

† Université de Paris-Sud.
‡ Université Montpellier II.

(1) Kresge, C. T.; Leonowicz, M. E.; Roth, W. J.; Vartuli, J. C.; Beck, J. S.; *Nature* **1992**, *359*, 710. Beck, J. S.; Vartuli, J. C.; Roth, W. J.; Leonowicz, M. E.; Kresge, C. T.; Schmitt, K. D.; Chu, C. T. W.; Olson, D. H.; Sheppard, E. W.; McCullen, S. B.; Higgins, J. B.; Schenker, J. L. *J. Am. Chem. Soc.* **1992**, *114*, 10834.
(2) Dabadie, T.; Ayral, A.; Guizard, C.; Cot, L.; Lacan, P. *J. Mater. Chem.* **1996**, *6*, 1789.
(3) Ogawa, M. *Chem. Commun.* **1996**, 1149.
(4) Bruinsma, P. J.; Hess, N. J.; Bontha, J. R.; Liu, J.; Baskaran, S. *Mater. Res. Soc. Symp. Proc.* **1997**, *443*, 105.
(5) Lu, Y.; Ganguli, R.; Drewien, C. A.; Anderson, M. T.; Brinker, C. J.; Gong, W.; Guo, Y.; Soyez, H.; Dunn, B.; Huang, M. H.; Zinks, J. I. *Nature* **1997**, *389*, 364.
(6) Klotz, M.; Ayral, A.; Guizard, C.; Cot, L. *J. Mater. Chem.* **2000**, *10*, 663.
(7) Kruk, M.; Jaroniec, M.; Sayari, A. *Langmuir* **1997**, *13*, 6267.
(8) Galarneau, A.; Desplantier, D.; Dutartre, R.; Di Renzo, F. *Microporous Mesoporous Mater.* **1999**, *27*, 297.
(9) Scherer, G. W.; Smith, D. M.; Stein, D. *J. Non-Cryst. Solids* **1995**, *186*, 309.
(10) Reichenauer, G.; Scherer, G. W. *J. Non-Cryst. Solids* **2000**, *277*, 162.
(11) Reichenauer, G.; Scherer, G. W. *J. Non-Cryst. Solids* **2001**, *285*, 167.
(12) Klotz, M.; Albouy, P.-A.; Ayral, A.; Ménager, C.; Grosso, D.; Cabuil, V.; Babonneau, F.; Guizard, C. *Chem. Mater.* **2000**, *12*, 1721.
(13) Impéror-Clerc, M.; Davidson, P.; Davidson, A. *J. Am. Chem. Soc.* **2000**, *122*, 11925.
(14) Edler, K. J.; Reynolds, A.; White, J. W.; Cookson, D. *J. Chem. Soc., Faraday Trans.* **1997**, *93*, 199.

10.1021/cm0211453 CCC: $22.00
Published on Web 06/29/2002

Table 1. Equations Used for the Calculation of Adsorbed N_2 Film Thickness, t

equation type	no.	parameters used (t in nm)	comments	ref
Halsey $t = a\left[\frac{b}{\ln(p/p_S)}\right]^c$	1	$0.343\left[\frac{-5}{\ln(p/p_S)}\right]^{1/3}$	adapted to silica, alumina, and clays	19
Harkins−Jura $t = \left[\frac{a'}{b' - \log(p/p_S)}\right]^{c'}$	2	$\left[\frac{0.1399}{0.034 - \log(p/p_S)}\right]^{1/2}$	general use	20
	3	$0.1\left[\frac{60.65}{0.030\,71 - \log(p/p_S)}\right]^{0.3968}$	established from experiments on MCM-41	7

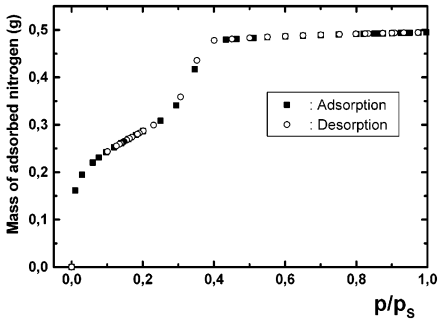

Figure 1. Nitrogen adsorption/desorption isotherm ($T = 77.4$ K); the vertical scale units are grams of adsorbed nitrogen per gram of powder.

The surfactant used to form the hexagonal mesophase was hexadecyltrimethylammonium bromide, $C_{16}H_{33}(CH_3)_3N^+,Br^-$. An acidic aqueous solution (10^{-2} M HCl) and ethanol (purity = 99.8%) were also used to prepare the gelling sol. The synthesis was carried out in two steps: TEOS, ethanol, and acidic water were first mixed in the molar ratio 1:6.75:8.2. The surfactant was then added at a molar ratio of surfactant to TEOS equal to 0.14. To obtain the final hexagonal powder, the gelling solution was poured into a wide beaker, resulting in a cracked thick layer after drying. The sample was first dried at room temperature for 12 h and then dried for 2 h at each 100, 150, and 175 °C in an oven. A thermal treatment to drive off the surfactant was carried out up to 450 °C under nitrogen. A second treatment was then applied under a flow of air to promote the elimination of residual organics. After calcination, the sample was ground to obtain the final powder.

Conventional Volumetric Measurements of Nitrogen Adsorption−Desorption. The analysis was carried out using a conventional volumetric apparatus (Micromeritics ASAP 2010). The evolution, as a function of relative pressure, of the adsorbed nitrogen mass per gram of powder at 77.4 K is shown in Figure 1.

From this isotherm, classical characteristics related to the porosity of the sample were first determined. The BET specific surface area was equal to 828 m^2/g.[15] The step associated with the capillary condensation in the cylindrical mesopores occurred at a relative pressure p/p_S of about 0.35, as expected for hexadecyltrimethylammonium bromide.[16] The absence of a hysteresis loop can be explained by a pore size less than 3.6−3.8 nm.[17] The average pore size was estimated using the BJH method.[18] Different equations giving the evolution as a function of p/p_S of the adsorbed N_2 film thickness, t (Table 1), were used.[7,19,20] The corresponding BJH pore sizes are reported in Table 2. They range from 2.7 to 3.4 nm. The flatness of the isotherm at high relative pressure indicates the absence of larger pores. The total pore volume determined from the adsorbed mass near saturation was found to equal 0.61 cm^3/g. From this value, a porosity of 57% was calculated assuming an amorphous silica density of 2.2 g/cm^3.[21]

Table 2. Porosity Characteristics as a Function of the $t(p/p_S)$ Equation Used[b]

$t(p/p_S)$[a]	average BJH pore size (nm)	ρ_W ($g\cdot cm^{-3}$)	wall porosity (%)	S_t ($m^2\cdot g^{-1}$)	R_P (nm)
1	2.7	1.51	32	274	1.76
2	2.7	1.48	33	286	1.73
3	2.8	1.58	28	290	1.82
3[b]	3.4	1.72	22	382	1.93

[a] cf. Table 1. [b] Using a corrected Kelvin equation with an additional term (+0.3 nm) for the BJH calculations.[7]

More information was extracted from the first part of the isotherm curve using a previously detailed calculation method.[6] Additional input data first had to be determined. The relative pressure corresponding to the starting point of the capillary condensation in the cylindrical mesopores, p/p_S^*, was equal to 0.175. It was obtained from the abscissa of the minimum of the curve before the capillary condensation peak on the derivative of the adsorption/desorption isotherm. The hexagonal parameter determined by X-ray scattering at room temperature, a, was equal to 5.456 nm. The output data (Table 2) are the silica wall density ρ_w, the surface area developed by the cylindrical mesopores S_t, and the radius of the cylindrical mesopores R_P. The wall density, ρ_w, ranges from 1.48 to 1.72 $g\cdot cm^{-3}$. The skeletal density of this kind of sol−gel-derived hexagonal silica was previously determined from He pycnometry measurements.[2] It is equal to that of dense amorphous silica (2.2 $g\cdot cm^{-3}$). These results are in agreement with the presence of open microporosity (pore size < 2 nm) inside the silica walls.[6] Such microporosity was also recently detected in hexagonal silica prepared under acidic conditions using other types of surfactants.[22] The calculated microporosity of the walls ranges from 22 to 31% as a function of the BJH method used. The additional surface associated with the microporosity corresponds to the difference between the BET specific surface area (828 m^2/g) and the surface area developed by the cylindrical pores, S_t (274−382 m^2/g, Table 2). The radius of the cylindrical mesopores, R_P, was in the interval 1.73−1.93 nm.

Nitrogen Adsorption Coupled X-ray Scattering. The X-ray setup consisted of a low-temperature diffractometer in the normal-beam lifting-detector geometry where the sample holder was rotated perpendicular to the incident beam. It was mounted on a rotating anode generator (copper anode, $\lambda = 0.1542$ nm) equipped with a doubly curved graphite monochromator. The sample holder was enclosed in a thermostated can whose internal gas pressure could be adjusted externally. The temperature range extended from 30 to 370 K. In the present experiments, the sample was held in a vacuum at 330

(15) Brunauer, S.; Emmett, P. H.; Teller, E. J. *J. Am. Chem. Soc.* **1939**, *60*, 309.
(16) Kruk, M.; Jaroniec, M.; Sayari, A. *J. Phys. Chem. B* **1997**, *101*, 583.
(17) Inoue, Y.; Hanzawa, Y.; Kaneko, K. *Langmuir* **1998**, *14*, 3079.
(18) Barret, E. P.; Joyner, L. G.; Halenda, P. H. *J. Am. Chem. Soc.* **1951**, *73*, 373.
(19) Cranston, R. W.; Inkley, F. A. *Advances in Catalysis and Related Subjects*; Farkas, A., Ed.; Academic Press: New York, 1955; Vol. 9, p 143.
(20) Lippens, B. C.; Linsen, B. G.; de Boer, J. H. *J. Catalysis* **1964**, *3*, 32.
(21) Iler, R. K. *The Chemistry of Silica*; Wiley: New York, 1979.
(22) Lee, J.-S.; Joo, S. H.; Ryoo, R. J. *J. Am. Chem. Soc.* **2002**, *124*, 1156.

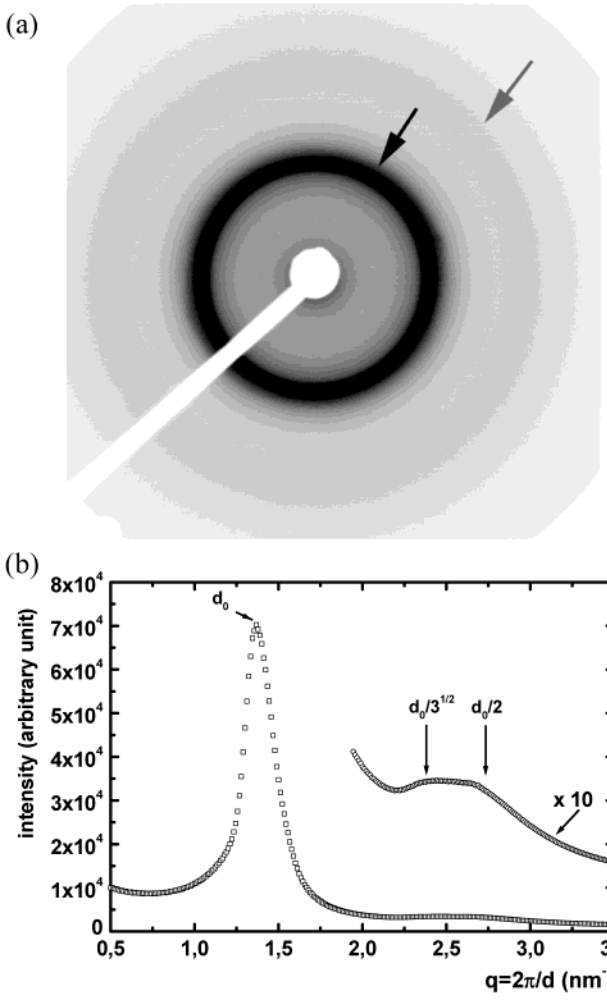

Figure 2. (a) X-ray diffraction pattern taken at room temperature; flat film geometry, sample to film distance = 730 mm. (b) Radial scan performed on the X-ray pattern in Figure 2a. In this type of scan, a point of abscissa q is obtained by integration of the intensity on a circle of radius q; it is characterized by a high sensitivity to weak diffraction features.

K for 1 h prior being cooled to 77.4 K. The mesoporous powder was contained in an unsealed glass capillary and maintained by a little cotton wadding; this precaution avoids unwanted powder displacement during gas admission. Absorption measurements require primary and transmitted intensities to be successively measured. For this purpose, the capillary was mounted slightly eccentrically on the sample holder so that it could be removed from the incident beam by a 90° rotation.

Diffracted intensities were recorded with a homemade linear detector that allows rapid line profile acquisition. It was replaced by a silicon diode for the absorption measurements, in which case the intensity levels were much higher. The diffraction pattern presented in Figure 2a was recorded on an imaging plate.

Results and Discussion

Absorption Data. The adsorption of gas into the pores of the silica samples is accompanied by a noticeable increase in beam attenuation; this effect must be properly estimated to correct diffraction data. Conversely, it is interesting to compute the expected absorption increase using the adsorption isotherm data and compare the expected value with the experimental result. Indeed, the attenuation of the X-rays is given by the relation $\exp(-\mu d)$, where μ represents the material linear attenuation coefficient and d is the sample thickness.[23] At any pressure, the coefficient μ is given by the relation

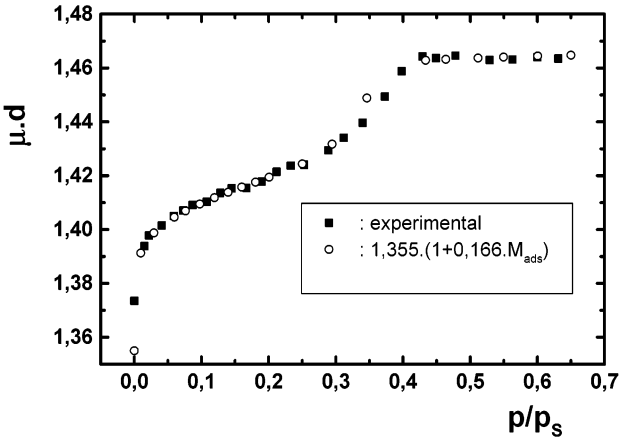

Figure 3. Pressure dependence of the sample X-ray absorption coefficient (T = 77.4 K); the open circles correspond to values calculated using the adsorption isotherm data

$$\mu = (\mu/\rho)_{SiO_2}\rho_{SiO_2} + (\mu/\rho)_{N_2}\rho_{N_2}$$

where μ/ρ represents the mass attenuation coefficient of the constituent considered (silica or nitrogen) and ρ is the constituent's density in the material. We thus have

$$\mu d \propto 1 + [(\mu/\rho)_N/(\mu/\rho)_{SiO_2}](\rho_{N_2}/\rho_{SiO_2})$$

The ratio ρ_{N_2}/ρ_{SiO_2} is equal to the mass of adsorbed nitrogen per gram of material, $m_{N_2}(p)$, and the mass attenuation factors are computed from the literature data[23] to give

$$\mu d \propto 1 + 0.196 m_{N_2}(p)$$

As shown in Figure 3, the experimental data are best adjusted with the equation

$$\mu d \propto 1 + 0.166 m_{N_2}(p)$$

In view of the errors involved in absorption measurements, the agreement can be considered acceptable.

Cell Parameter and Correlation Length. The diffraction pattern shown in Figure 2a was recorded at room temperature and essentially consists of two diffraction rings (see arrows); a radial scan plotted in Figure 2b indicates that (i) the first-order line corresponds to a d spacing of d_0 = 4.715 nm and (ii) the weaker ring cannot be attributed to a single diffraction line. Indeed, assuming a 2D hexagonal structure, this ring can be separated into the contributions of lines located at $d_0\sqrt{3}$ [Miller indexes (1,1) or (2,−1)] and $2d_0$ [Miller indexes (2,0) or (2,−2)]. The hexagonal parameter is deduced from the relation $a = d_0 2/\sqrt{3}$, which leads to a value of 5.456 nm at room temperature.

In the following discussion, lattice parameter measurements were performed with a linear detector that permits relative changes of the first-order ring diameter

(23) *International Tables for Crystallography*; International Union of Crystallography: Chester, U.K., 1995; Vol. C, p 182.

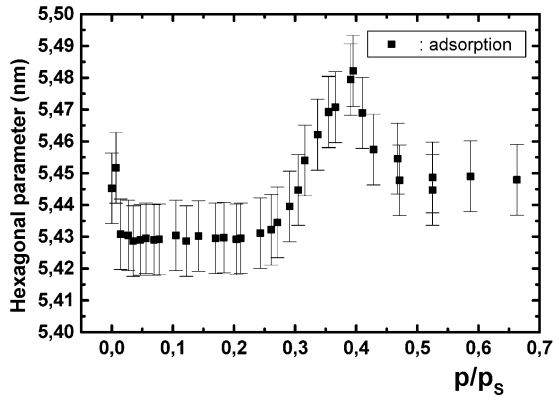

Figure 4. Pressure dependence of the 2D hexagonal parameter ($T = 77.4$ K).

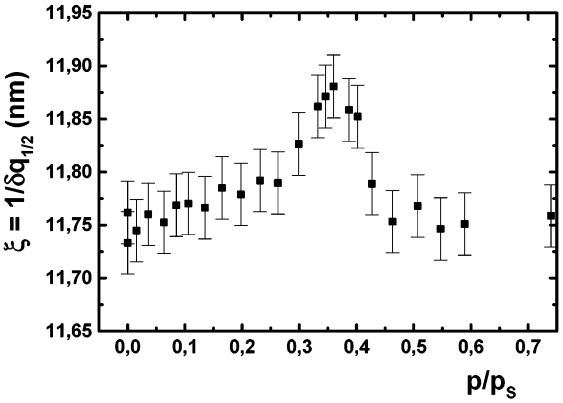

Figure 5. Pressure dependence of the domain correlation length ($T = 77.4$ K).

to be measured with a precision of ca. 0.1%. Upon cooling to 77.4 K, a thermal contraction of about 0.2% is observed to compare with nearly zero contraction in bulk amorphous silica. The behavior of the hexagonal parameter during gas adsorption is plotted in Figure 4. A small contraction is first observed at very low pressure, followed by a stabilization. More surprising is the parameter increase associated with the capillary condensation. As previously discussed, a contraction was expected to be associated with the capillary stresses applied by liquid nitrogen menisci on the pore walls.[9−11] No explanation is proposed for this effect whose amplitude remains limited.

The line profile was also analyzed to estimate the domain correlation length ξ, i.e., the distance over which positional correlations are maintained between cylindrical pores. A Lorentzian profile was found after correction for resolution, characterized by a half-width at half-intensity of $\delta q_{1/2}$; the correlation length associated with this type of line broadening is $\xi \approx 1/\delta q_{1/2}$.[24] The experimental values are plotted in Figure 5 and amount to about twice the hexagonal parameter. This means that important fluctuations in the pore positions occur that lead to a rapid loss of positional order. The slight increase of ξ observed during capillary condensation is quantitatively related to the increase of the hexagonal parameter in the same region.

Diffracted Intensity. *Diffraction Equation.* Before diffraction data are discussed, some equations should be briefly reviewed.[13] In a 2D hexagonal powder, the diffracted intensity associated with lines of indexes (h,k) is given by

$$I(\vec{q}_{h,k}) = KM(h,k)\frac{|F(\vec{q}_{h,k})|^2}{q_{h,k}^{\ 2}}$$

where the modulus of the scattering vector $\vec{q}_{h,k}$ is

$$q_{h,k} = (4\pi/a\sqrt{3}\sqrt{h^2 + k^2 + hk})$$

$F(\vec{q}_{h,k})$ represents the structure factor, that is, the Fourier transform of the electron density in the unit cell. $M(h,k)$ and $1/q_{h,k}^2$ are the line multiplicity and the Lorentz factor, respectively. Absorption corrections are included in the multiplying factor K and comprise a sample contribution in the form $\exp(-\mu d)$ and the beam attenuation due to the gaseous nitrogen present in the can.

The evaluation of the structure factor

$$F(\vec{q}_{h,k}) = \int\int_{\text{unit cell}} \rho^{\text{el}}(\vec{r})\, \exp(i\vec{q}_{h,k}\vec{r})\, \mathrm{d}^2 r$$

is facilitated by noticing that an arbitrary constant can be added to the electron density without changing its value except at $\vec{q} = 0$. If the wall electron density $\rho^{\text{el}}_{\text{wall}}$ is assumed to be constant, one can write

$$F(\vec{q}_{h,k}) = \int\int_{\text{unit cell}} (\rho^{\text{el}}(\vec{r}) - \rho^{\text{el}}_{\text{wall}})\, \exp(i\vec{q}_{h,k}\vec{r})\, \mathrm{d}^2 r$$

Assuming further that the pore cross section is circular, polar coordinates can be used, leading to the expression

$$F(q_{h,k}) = \pi\int_0^{R_{\text{P}}} [\rho^{\text{el}}(r) - \rho^{\text{el}}_{\text{wall}}) J_0(q_{h,k}r)\, r\mathrm{d}r$$

where R_{P} represents the pore radius and J_0 is the Bessel function of order 0. Alternatively, the mathematical relation $(\mathrm{d}/\mathrm{d}z)[zJ_1(z)] = zJ_0(z)$ can be used to derive the equation

$$F(q_{h,k}) = -\frac{\pi}{q_{h,k}}\int_0^{R_{\text{P}}} rJ_1(q_{h,k}r)\,\frac{\mathrm{d}\rho^{\text{el}}(r)}{\mathrm{d}r}\,\mathrm{d}r \qquad (1)$$

where J_1 is the Bessel function of order 1.[25] This last expression clearly exposes the role of variations in the electron density in the diffraction process.

Experimental Results. The behavior of the first-order peak intensity was precisely evaluated during an adsorption/desorption cycle and is displayed in Figure 6. Before considering this curve in detail, it is worth looking at the intensity behavior of the higher-order diffraction lines. For this purpose, the weak diffraction ring observed at higher angle in Figure 2a,b was analyzed in terms of two lines of fixed d spacings, $d_0\sqrt{3}$ and $2d_0$. To facilitate the computation, similar widths were attributed to the two peaks. Indeed, this parameter was found to be larger than for the first-order peak by a factor 1.7, which constitutes additional evidence for positional disorder. The peak intensities normalized to the first-order peak intensity are plotted in Figure 7a

(24) Langford, J. I.; Louër, D.; Scardi, P. *J. Appl. Cryst.* **2000**, *33*, 964. Langford, J. I.; *J. Appl. Cryst.* **1978**, *11*, 10.

(25) Watson, G. N. *Theory of Bessel Functions*; Cambridge University Press: Cambridge, U.K., 1958.

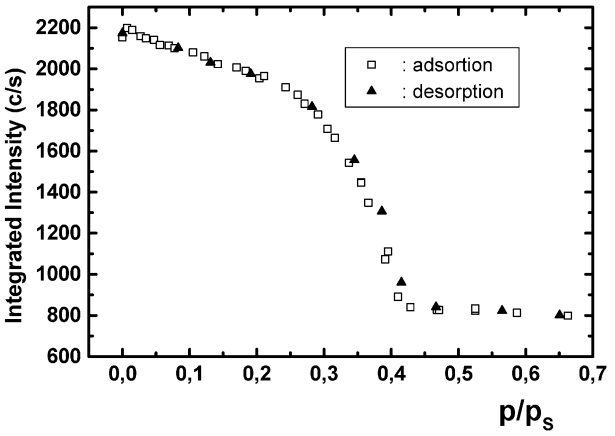

Figure 6. Pressure dependence of the first-order line intensity ($q_{10} = 4\pi/a\sqrt{3}$;T = 77.4 K). The data are corrected for absorption effects.

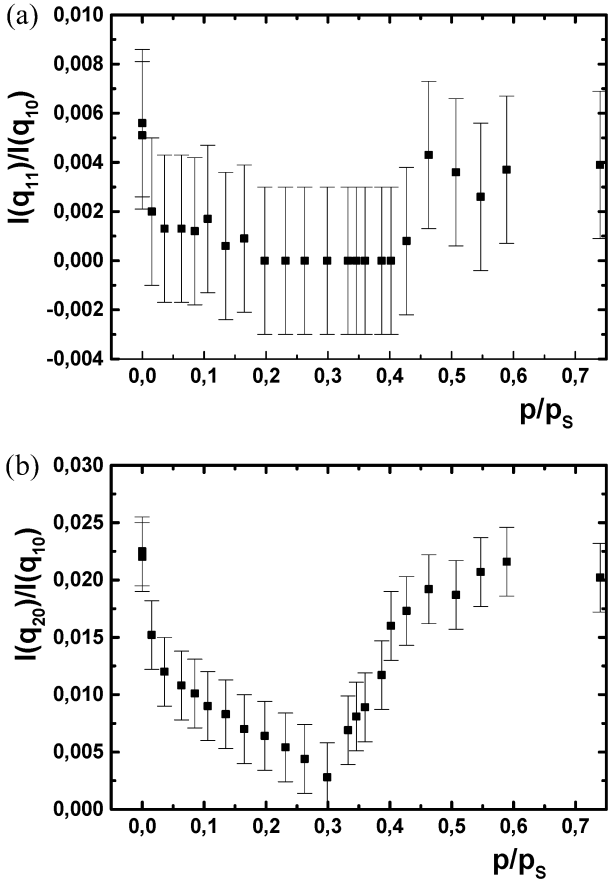

Figure 7. (a,b) Pressure dependence of the ratio of the intensity of the higher-angle diffraction lines ($q_{11} = 4\pi/a$ and $q_{20} = 8\pi/a\sqrt{3}$) to the intensity of the first-order line ($q_{10} = 4\pi/a\sqrt{3}$). Notice that similar values are found at zero pressure and after capillary condensation for both diffraction lines.

and b. Two important points are noticeable: First, the values observed before gas entrance and after capillary condensation are very similar. In other words, the structure factors differ only by a multiplicative factor in both situations. Referring to eq 1, this observation suggests that the variations in electron density can be modeled in a similar way when the pores are empty or filled. Second, a dramatic change in the intensity ratios is observed just after gas admission; this indicates a change in the electron density repartitioning in the intermediate situation.

Model I (One Step). This simple model is used to describe the electronic density before adsorption and after capillary condensation. The wall density is assumed to be constant, although previous studies have demonstrated the existence of a lower-density layer surrounding the pores.[14,26] Indeed, such structural features essentially affect higher-order diffraction lines, which cannot be observed in the present sample.[13,14] The electron density is thus described by a single step between mesopores and walls, and its derivative is given by $(\rho^{el}_{pore} - \rho^{el}_{wall})\delta(r - R_P)$; the integral in eq 1 is readily computed as

$$F(q_{h,k}) = \pi R_P^2(\rho^{el}_{pore} - \rho^{el}_{wall})\frac{J_1(q_{h,k}R_P)}{q_{h,k}R_P}$$

Before absorption, the wall electron density is written as

$$\rho^{el}_{wall} = (1 - \Pi)\rho^{el}_{SiO_2}$$

where Π indicates the degree of microporosity and $\rho^{el}_{SiO_2}$ is the electron density of the silica skeleton; the pore density is zero. After capillary condensation, the densities are modified to

$$\rho^{el}_{wall} = (1 - \Pi)\rho^{el}_{SiO_2} + \Pi\rho^{el}_{N_2L}$$

and

$$\rho^{el}_{pore} = \rho^{el}_{N_2L}$$

where $\rho^{el}_{N_2L}$ represents the electron density of liquid nitrogen. As the lattice periodicity remains almost constant throughout the condensation process, the factor $J_1(q_{h,k}R_P)/q_{h,k}R_P$ is unchanged. The ratio of the diffracted intensity after condensation and at zero pressure is thus equal to $(1 - \rho^{el}_{N_2L}/\rho^{el}_{SiO_2})^2$ and does not depend of the microporosity percentage; the experimental value of this ratio is 0.376. Assuming the mass density of liquid nitrogen in the material to be similar to the bulk value $\rho_{N_2L} = 0.807$ g/cm^3, a mass density of $\rho_{SiO_2} = 2.15$ g/cm^3 is obtained for the skeleton of the silica walls. (Care must be taken not to confuse density and electron density, which are simply related by a factor involving molar mass and atomic number.) This result is in close agreement with data found in the literature for amorphous silica, ca. 2.2 g/cm^3.[21]

The pore radius R_P can also be evaluated using the results presented in Figure 7a,b. Indeed, the intensity ratio between the first diffraction line and a reflection of indexes (h,k) is given by

$$\left(\frac{q_{1,0}R_P}{J_1(q_{1,0}R_P)}\frac{J_1(q_{h,k}R_P)}{q_{h,k}R_P}\right)^2$$

where all factors are known except for R_P. Satisfying agreement with the experimental values is found for a pore radius of 1.79 nm, as shown in Table 3. This value

(26) Edler, K. J.; Reynolds, A.; White, J. W. *J. Phys. Chem. B* **1998**, *102*, 3676.

Table 3. One-Step Model: Experimental and Calculated Intensity Ratios

intensity ratio	I_{11}/I_{10}	I_{20}/I_{10}
experimental determination	0.0041	0.021
calculation ($R_P = 1.79$ nm)	0.0056	0.019

falls within the interval determined from the adsorption isotherm, 1.73−1.92 nm (Table 2). The wall microporosity deduced from this estimation of the pore radius is $\Pi = 0.28$ (which corresponds to ca. 30% of the total adsorbed nitrogen mass).

Model II (Two Steps). As previously explained, an adsorbed film is expected to form at the surface of both micro- and mesopores after gas admission. In that case, the electron density can be modeled by two steps corresponding to the transition between the inner part of the mesopore and the adsorbed film on one hand and between the adsorbed film and the wall on the other. Its derivative is now given by $(\rho^{el}_{wall} - \rho^{el}_{N_2L})\delta(r - R_p) + \rho^{el}_{N_2L}\delta(r - R_P + t)$, where t is the thickness of the film lining the mesopores. The density of the adsorbed film is further assumed to be similar to the nitrogen bulk value. Under these conditions, the structure factor is given by the more complex equation

$$F(q) = \pi(R_P - t)^2\rho^{el}_{N_2L}\frac{J_1[q(R_P - t)]}{q(R_P - t)} + \pi R_P{}^2(\rho^{el}_{wall} - \rho^{el}_{N_2L})\frac{J_1(qR_P)}{qR_P} \quad (2)$$

This equation is of course similar to that given for model I in the two limits of empty pores ($t = 0$) and completely filled pores ($t = R_P$). However, the model is not valid during capillary condensation, where a statistical distribution between completely and partially filled mesopores should be introduced. At any pressure, the total amount of adsorbed gas, $m_{N_2}(p)$, is known from the adsorption isotherm and can divided into two parts: one corresponding to the fraction adsorbed into the mesopores, $M^{meso}_{N_2}(p)$, and the other associated with the microporosity, $M^{micro}_{N_2}(p)$. The structure factor in eq 2 is entirely determined by the knowledge of one of these two masses by elementary algebra, assuming that the pore radius and the wall microporosity are known. In turn, the pressure dependences of $M^{meso}_{N_2}(p)$ and $M^{micro}_{N_2}(p)$ can be deduced from the intensity variations of the first-order diffraction peak displayed in Figure 6; the results are plotted in Figure 8 (the calculations were performed with a pore radius of $R_P = 1.79$ nm and a wall microporosity of $\Pi = 0.28$). As mentioned above, the model is no longer valid during capillary condensation, and the calculated masses must be considered as qualitative in this range. It is first seen that $M^{micro}_{N_2}(p)$ reaches an equilibrium value at a relatively high pressure ($p/p_S \approx 0.35$), which indicates the presence of large pores in the walls. At lower pressures, the two masses display remarkably similar behaviors. The pressure dependence of the film thickness t [deduced from $M^{meso}_{N_2}(p)$] is plotted in Figure 9, where it is compared with the different equations given in Table 1. Equation 3 of the Harkins−Jura type, whose parameters were deduced from experiments on MCM-41, accounts quite well for the experimental data up to relative pressures

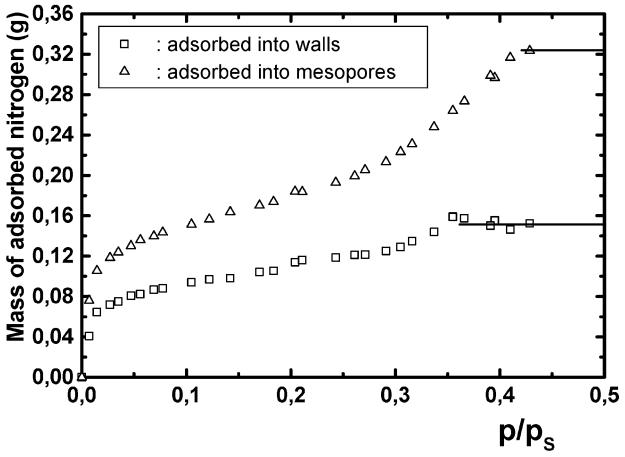

Figure 8. Pressure dependence of the nitrogen mass (per gram of powder) adsorbed into the micropores and into the mesopores as deduced from model II. The lines indicate the asymptotic values.

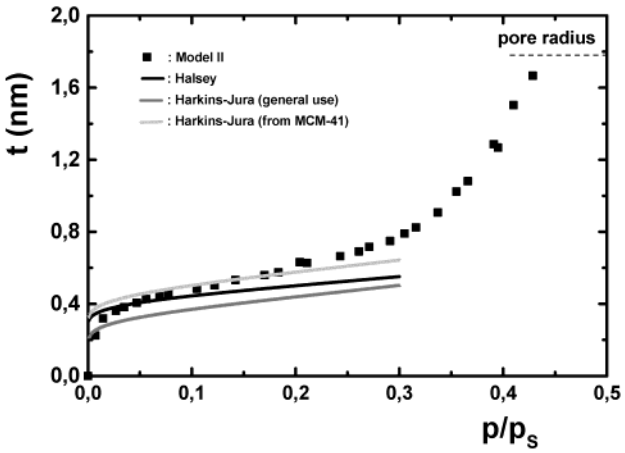

Figure 9. Pressure dependence of the nitrogen layer thickness adsorbed onto the pore walls according to model II. The solid curves correspond to the predictions by the various $t(p/p_S)$ equations used.

ca. 0.2. The rapid increase observed above this value corresponds to the onset of capillary condensation where the model is no longer valid.

Conclusions

Simple X-ray diffraction techniques are associated with gas adsorption measurements for the study of a 2D hexagonal mesoporous silica powder. Our primary goal was to detect possible material shrinkage induced by capillary condensation; it is shown that, contrary to expectations, a slight sample expansion is observed. Furthermore, the contrast variations in electron density due to the adsorption process lead to a drop in scattered intensity that can be easily measured. The density of the wall skeleton can be deduced directly from the amplitude of this decrease. A closer analysis of the data allows the fractions of nitrogen adsorbed into the micropores and into the mesopores to be separated using a very simple electron density model. The occurrence of rather large pores in the walls is confirmed. An estimation of the film thickness lining the pores before capillary condensation is in good agreement with the prediction of a specially modified Harkins−Jura equation.

Now, it will be interesting to apply this method for the characterization of MCM-41 samples (hydrothermal synthesis under basic conditions) whose well-ordered structure allows a larger number of diffraction lines to be observed. The wall density can be estimated and compared with that of ordered silica obtained under acidic conditions. Using X-ray scattering and small-angle neutron diffraction, Edler et al.[14,26] investigated the wall structure of MCM-41 samples, which is highly dependent on the synthesis conditions and on the further thermal treatment; an estimation of the microporosity of the zones of different densities introduced in their model could be possible. Extension to the characterization of other ordered mesoporous oxides prepared under various conditions is also very interesting.

Some tests not presented here were performed using argon instead of nitrogen. The markedly higher electron density of this element in the liquid state dramatically amplifies the changes in diffracted intensity. By choosing an appropriate gas, it is thus possible to adapt the contrast between the walls and the condensate; this might be useful for the study of mesoporous materials containing heavier elements such as titanium or zirconium. This point recalls the technique of contrast variation commonly used in neutron scattering.[26,27]

Indeed, the results presented in this paper were obtained using bulk powder samples. However, the method appears very attractive for the characterization of the porosity of ordered thin films for which the nitrogen adsorption analysis using conventional volumetric method is complex.[28] In that case, additional information including the film density and thickness can be drawn from an analysis of the reflectivity data.

CM0211453

(27) Ramsay, J. D. F.; Kallus, S. J. *J. Non-Cryst. Solids* **2001**, *285*, 142.
(28) Ayral, A.; El Mansouri, M.-P.; Vieira, C.; Pilon, C. *J. Mater. Sci. Lett.* **1998**, *17*, 883.